

# Design of a Non-Flapping Morphing Drone Inspired by the Western Gull

Jose Aguilera Fuentes, Jeffrey Astorga, Marco Zuloaga, Jeremy LeMaster, Adrian G. Corral, Jonathan Balan, Joseph Mackey de Zela, Matthew Emil Martin, Harmandeep Gill, Brianna Murphy, Jesus Soloman, John Cannon, Thomas Helo

and

Peter L. Bishay

*Department of Mechanical Engineering, California State University, Northridge*

Since the inception of flying vehicles, inventors have been inspired by various kinds of birds. However, a lot of characteristics of avian flight are yet to be replicated in drones and commercial airplanes. Bio-inspiration from birds can lead to improvements in maneuverability, efficiency, and adaptability of flying vehicles at various flight conditions. This work presents the design and analysis of “BIRD” (Bio-Inspired Reconfigurable Drone), a non-flapping drone with bioinspired morphing capabilities in both its wings and tail. The shape and size of all components were inspired by the western gull. BIRD features pitch and coupled sweep-span morphing capabilities in its wings, along with pitch and tilt morphing in the tail, to achieve higher efficiency in a broader range of flight phases and attitudes than fixed-wing aircraft. Various approaches were utilized to reduce the drone’s weight including the use of composite materials in creating the structural components, and the design of double and triple feather groups with a common feather shaft. A sensor system that tracks the dynamic forces and flight performance was integrated in the design. Computational models were developed to guide the design process. A proof-of-concept model was manufactured, and various tests were performed to validate the design decisions.

## I. Introduction

Flight pioneers were deeply inspired by the natural flight of birds, which served as the foundation for many of their designs and concepts. Early aviation pioneers, like Leonardo da Vinci, studied bird flight carefully, noting how birds’ wings generated lift and how their bodies maneuvered through the air [1]. The Wright brothers applied these principles when designing their first successful airplane. They experimented with gliders and controlled flights, taking inspiration from birds’ ability to twist and adjust their wings to maintain control [2]. Otto Lilienthal, the German aviation pioneer, made detailed observations of birds in flight and incorporated similar techniques into his own glider designs. His work demonstrated the importance of wing shape and aerodynamics, which were directly influenced by avian flight [3]. This bird-inspired approach to flight laid the groundwork for the technological advancements that led to modern aviation. However, a lot of avian flight characteristics have been only carefully studied recently with the aid of state-of-the art technologies. With the current advances in microelectronics, wireless communication, additive manufacturing, and composite materials, new designs of bio-inspired drones can be created, resuming the efforts of early pioneers.

Flapping and non-flapping morphing drones represent two cutting-edge approaches to the development of unmanned aerial vehicles (UAV), each with unique advantages and challenges [4]. Flapping drones, often inspired by birds and insects, use flexible wings that mimic the motion of natural flight, enabling them to achieve greater maneuverability at low Reynold’s numbers. These drones can perform complex aerial tasks like hovering, dynamic turns, and tight maneuvers that non-flapping drones struggle with at low speeds [5]. Non-flapping morphing drones, on the other hand, rely on rigid wing structures that can change shape or configuration during flight, allowing for adaptability in various flight conditions. For instance, wing morphing can help optimize the aerodynamics at different speeds and altitudes [6]. Both types of drones, whether flapping or non-flapping, are pushing the boundaries of aerial technology, aiming to mimic

the efficiency and versatility of natural flyers while overcoming the technical limitations of traditional rigid-wing aircraft. Avian-inspired UAVs can provide new insights to researchers studying bird flight [7]. Studying avian flight is also significantly inspiring new drone designs with high efficiency, stability, and maneuverability [8,9]

Various bio-inspired non-flapping morphing wings, tails, and full drones have been developed recently. For example, Kilian *et al.* [10] developed a morphing wing inspired by crow wings. The rachides were made of carbon fiber reinforce polymer (CFRP) sheets, whereas the remiges and covert vanes were made of 0.3 mm thick polystyrene (PS) sheets. Murayama *et al.* [11] developed and tested a feathered tail with tilt, pitch, and tail-spread capabilities to produce pitch and yaw moments. Li *et al.* [12] developed a feathered tail mechanism capable of mimicking nearly all movements observed in real bird tails. Gamble and Inman [13] used macro fiber composite (MFC) actuator to design a multi-functional morphing control surface based on the horizontal tail of birds. Yaw and pitch control, along with limited air break control were achieved as a result of the bend-twist coupling of the composite. Di Luca *et al.* [14] used artificial feathers in their morphing wing and showed that fully deployed configuration enhances maneuverability while folded configuration offers low drag at high speeds. Hui *et al.* [15] designed a morphing discrete wing, inspired by the pigeon's wing. They showed that discrete, or feathered, wing surface can achieve an induced drag reduction through decreasing the wing-tip vortex strength seen in continuous wings, while also improve the lateral stability of the UAV. The design of LisHawk [16] was inspired by the northern goshawk, and it possessed an ability to change the area of its wings and tail using feather spreading mechanism, along with tail pitch and yaw degrees of freedom (DOF). LisEagle [17] was inspired by the eagle's flight and added the wing pitch DOF to the drone's morphing capabilities. PigeonBot [18] was inspired by the pigeon and possessed real pigeon feathers that can spread to change the wing area. PigeonBot II [19] also included natural feathered wings that can spread and a tail that can spread, elevate, tilt, and deviate side to side like a bird. MataGull [20,21] was inspired by the seagull and included flexible mechanisms for spreading the wing and tail feathers, along with a tail that can tilt and pitch. CGull [22,23] was also inspired by the seagull and featured lightweight composite feathers that are actuated using a linkage mechanism.

This paper presents a bio-inspired non-flapping morphing drone, named "BIRD" (Bio-Inspired Reconfigurable Drone), under the biomimetic shape and size of the western gull, *Larus Occidentalis*. BIRD features two coupled morphing degrees of freedom in the wings: wing spread and wingtip pitching, a combination that has not been realized in any bio-inspired drone in the literature so far. Wing morphing alters the generated lift and drag forces, as well as the pitch and roll moments. BIRD's tail has two independent degrees of freedom, pitch and tilt, to control the pitch and yaw moments. The rest of the paper is organized as follows: the preliminary computational model that was developed in MachUpX, along with its results, are presented in the next section. This is followed by the model description, and avionics and propulsion systems. Manufacturing details come next, followed by preliminary testing.

## II. Computational Modeling

A simplified model of a gliding western gull was first developed in the open-source software MachUpX to study the effect of all morphing degrees of freedom on the generated aerodynamic forces and moments. This numerical tool is based on the lifting line theory and does not require generation of an intensive mesh as in the case of finite volume and element analysis tools. Hence, computational times are significantly shorter, enabling the performance of larger number of simulations at various morphing configurations. **Fig. 1** shows the simplified model in extended and tucked configurations. Since the fuselage does not significantly contribute to the aerodynamic forces and moments, the computational model has no fuselage. The model has inner, middle, and outer wing sections, where the inner and outer sections sweep back in the tucked configuration, while the middle wing section sweeps forward. Most of the geometric dimensions of the model match the average dimensions of the western gull [24]. The span of the model in extended and tucked configurations are 1.32 m and 1.12 m, respectively. The length of the model is 0.72 m, and the chord length of the wing is 0.29 m. The distance separating the wing and tail was set to 0.24 m. A reduction of 15% in wing area is achieved when the drone transforms to a tucked configuration. Selig 1223 airfoil was assigned to the profiles of the inner and middle wing segments as well as the tail. The outer wing profile was NACA 0006 to represent feathers at the outer wing. The tail is oriented such that it produces downforce (or negative lift), rather than lift, in order to maintain longitudinal stability and create a positive pitching moment so that the wings can be oriented at a higher angle of attack (AOA). The target weight was 1,250 g which matches the maximum weight of the western gull. However, during the

design and manufacture of the first iteration of the drone (BIRD I), it was realized that the actual final weight was much closer to 2,500 g—therefore, MachUpX simulations were rerun with the more accurate weight value in order to obtain more trustworthy moment values. BIRD II and BIRD III were also simulated with as-measured weights for maximum accuracy. Various models were also made of the Western Gull itself in order to have a performance benchmark which could be used to evaluate the degree to which we fulfilled our original objectives of biomimicry and the maneuverability which stems from it. In order to ensure all simulations' data could be compared, the following parameters were defined for all models of BIRD as well as Western Gull: fluid density of  $1.225 \text{ kg/m}^3$ , temperature of 288.16 K, viscosity of  $1.78994 \times 10^{-5} \text{ kg/(m.s)}$ , standard atmospheric pressure, and the velocity was set to  $12.07 \text{ m/s}$  (27 mph), which is about 30% lower than the maximum speed that western gull can achieve,  $15.65 \text{ m/s}$  (35 mph) [24].

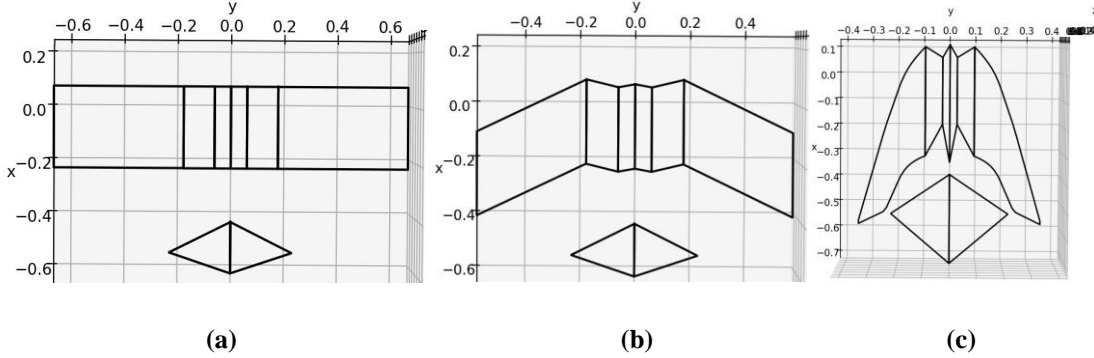


**Fig. 1. MachUpX models of BIRD (a) fully extended, (b) fully tucked configuration as well as a (c) fully tucked model of the Western Gull (unit: m)**

The considered range of AOA in all studies is  $-5^\circ$  to  $12^\circ$ ; no roll or yaw were included in any MachUpX simulation for the sake of direct comparison ability. **Fig. 2a** shows the generated lift force vs. AOA at the extended and tucked configurations with and without wingtip and tail pitch, modeled with BIRD I parameters. It can be seen that at positive angles of attack the extended wing configuration increases the generated lift and the wingtip and tail pitch further increase the generated lift.

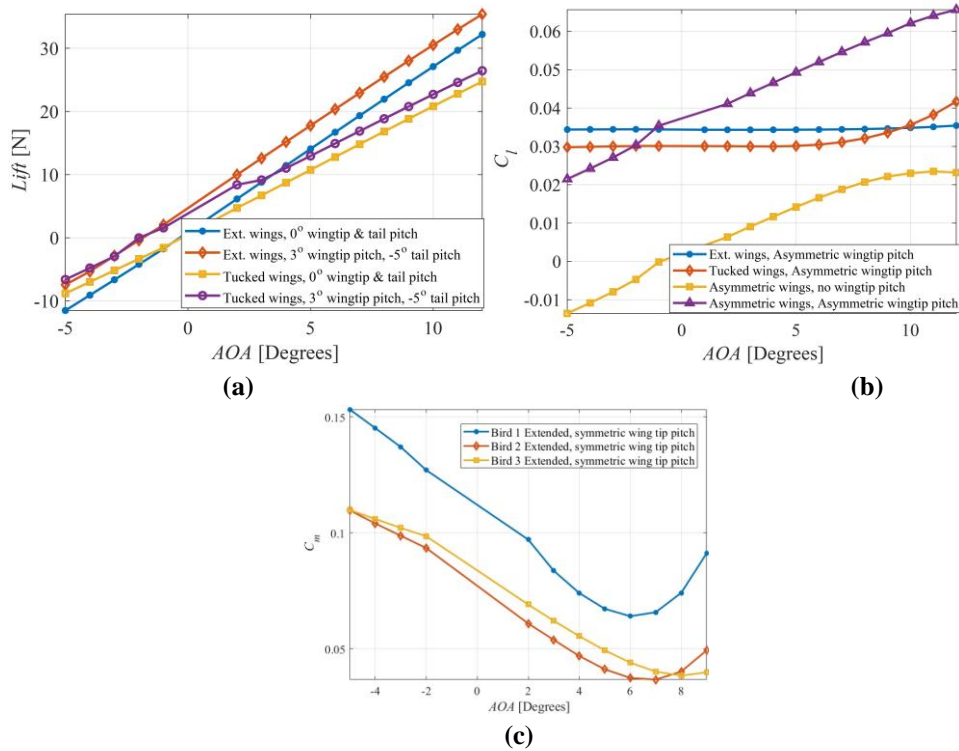


**Fig. 2. (a) Lift, and (b) roll moment coefficient, vs. AOA for various wing and tail configurations (BIRD I iteration); pitch moment coefficient vs. AOA for all three iterations of BIRD**

**Fig. 2b** shows the roll moment coefficient,  $C_l$ , vs. AOA when the wingtip pitch is asymmetric (left wing is at  $3^\circ$ , and right wing is at  $-3^\circ$ ), and when the wing sweep is asymmetric (left wing extended, and right wing tucked). These simulations were also performed using the BIRD I model and original target weight of 1,250 g. It can be seen that asymmetric wingtip pitch on both extended and tucked wings has more control authority over asymmetric wing sweep. This is in agreement with the findings of Ajanic *et al.* [17] on LisEagle. Combining both asymmetries can enhance the roll moment coefficient significantly at higher AOA. **Fig. 2c** shows us that the original version of the drone had the highest pitch authority, likely due to the fact that it had the largest wing area of the three drones, most critically and especially at the feathered portion of each wing, which is the portion that pitches in a manner similar to ailerons on a conventional aircraft. BIRDS II and III have much more closely-spanned feathered wing segments, and therefore display nearly identical curves. It is worth noting that all three curves have the same shape, despite the fact that BIRD I's pitch coefficient is consistently higher than the other two drones' for any angle of attack—this is a desirable aerodynamic trait, as it makes the pilot's transition from one drone to another seamless, and they do not have to alter their expectations and control methods regarding how a given input would affect the drone's attitude from one drone to the next. This similarity in aerodynamic characteristics is complemented mechanically by the fact that the center of gravity did not shift significantly between BIRDS despite drone dimensions and weight both shrinking.

**Fig. 3** captures the comparison between the three iterations of BIRD and how closely the drones' values emulate those of the real Western Gull—all three iterations of BIRD were similar in aerodynamic performance to one another, which was a desirable accomplishment given the fact that wing area was steadily decreasing from iteration to iteration. The primary reason why successive iterations did not suffer aerodynamically stemmed from the fact that much of the eliminated portion of the span was from the feathers, which were flat and did not contribute much at all toward useful force generation due both to their lack of pressure gradient produced by their cross-section, and the fact that they could only pitch about five degrees before stalling. Lift was also maintained from iteration to iteration despite span changes by increasing the chord length of the inner (Selig 1223) wing segments in proportion to their span decrease—this largely compensated for the span shrinkage's lift loss, at least in the simple software. In reality, the migration towards lower aspect-ratio wing segments, particularly with the gaps present between segments which are necessary for tucking, would likely produce larger and larger tip-vortex-induced losses. This effect could not be modeled in MachUpX since no gaps between segments could be modeled, as the universal joints used on the real drone cannot be modeled in the software, and approximating their effect while retaining the gap by using extremely short-chord airfoils in their place would have likely produced many errors.

The work with ANSYS Fluent began with a self-guided learning phase, which foundational skills were developed by watching YouTube tutorials on 2D airfoil simulation. This early learning phase helped develop familiarity with the interface of the program in terms of meshing procedures, boundary condition setup, solver configurations, and result interpretation. Following this, simulations were advanced to 3D airfoils to gain experience in more complex geometries and flow dynamics. After becoming proficient with the software, simulating the tail section of the UAV was then assigned. While the geometry and simulation setup were completed, there were difficulties obtaining accurate or converged results, despite multiple attempts to adjust simulation parameters. The simulations were then shifted to focus on a simplified version of the full UAV model. This simplified model removed non aerodynamic components such as internal fuselage features, out feathers, wing covers, and the motor and propeller. The components were merged to create smoother transitions between geometry elements. The first iteration included a simplified fuselage, tail, and symmetric rectangular wings. In the second iteration, the wings were separated into inner, middle, and outer wing sections to more closely replicate the actual UAV's structure. The Selig 1223 was used for the inner and middle wing section along with the revolved tail. Later iterations added geometry that replicated the feathers to the outer wings but due to meshing and solver instability, the wings were merged into a continuous surface and the features were omitted to produce a cleaner more meshable geometry similar to the first version.

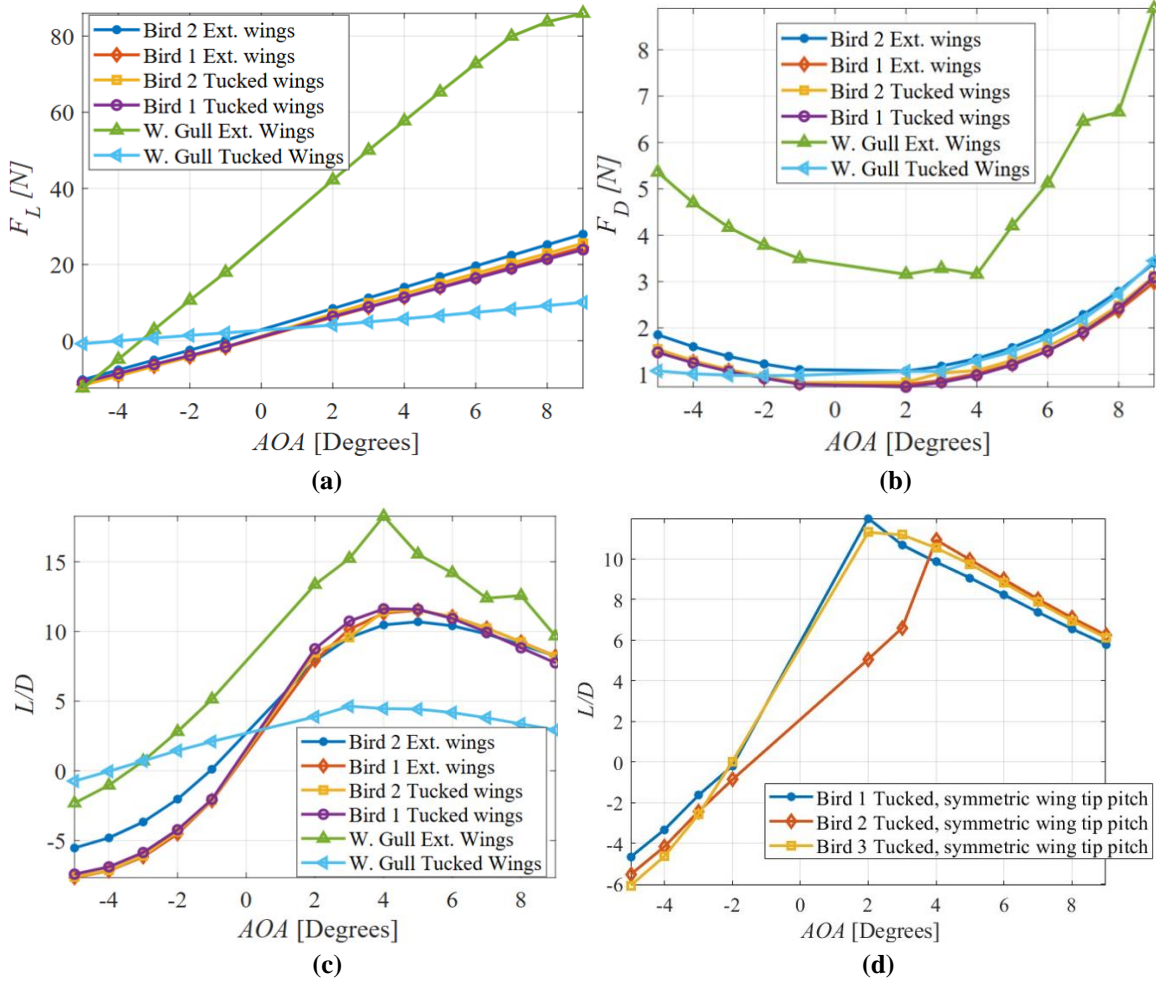


**Fig. 3. Comparisons of lift (a), drag (b), and efficiency (c) between BIRDS I and II and the Western Gull with both fully extended and fully tucked wings, as well as efficiency of the three BIRDS compared to each other (d)**

Over the course of four major iterations, contributions to the refinement of the geometry and meshing were made. The simulation domain was created by adding a 1.3-meter enclosure in all directions and extending 3.5 meters in the positive x direction to simulation freestream flow. A Boolean operation was used to subtract the UAV geometry from the enclosure, creating a proper fluid domain for the external flow simulations. Different meshing approaches were also utilized including adding inflation layers to capture boundary layer effects and switching mesh types such as hex-dominant and tetrahedral elements to improve mesh quality and solver stability.

The effect of tail tilt pitch on the pitch and yaw moment coefficients is shown in Fig. 4 and Fig. 5, respectively. Increasing the tail pitch angle leads to a higher pitching moment coefficient, whereas increasing the tail tilt angle reduces the pitching moment coefficient in a nonlinear manner. The magnitude of the yaw moment coefficient increases as the tail tilt increases, and this effect is enhanced as the tail tilt angle increases.

CFD simulation efforts in Ansys did not yield converging results. The most recent simulations were performed on simplified models generally representing the recent iteration of BIRD. Fig. 4 shows the simplified model of BIRD in its fully extended wing configuration that was used for Ansys modeling. This model omitted much of the details of BIRD and instead featured simplified wing profiles in an attempt to significantly reduce the complexity of the geometry of the full CAD assembly. Another simplified model shown in Fig. 5 shows the simplified model of BIRD in its fully tucked configuration.

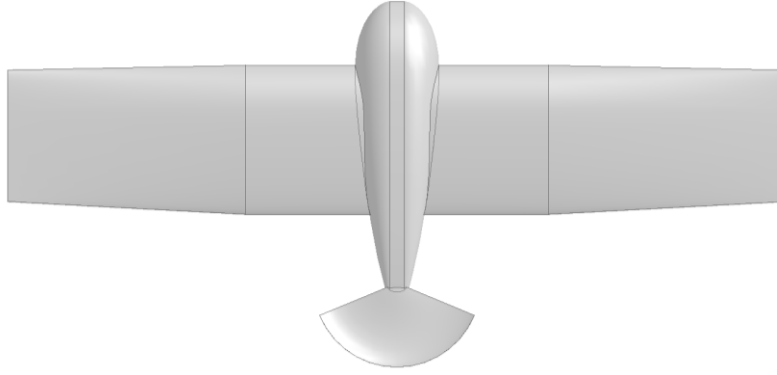


**Fig. 4. Simplified model of BIRD, fully extended wing configuration**

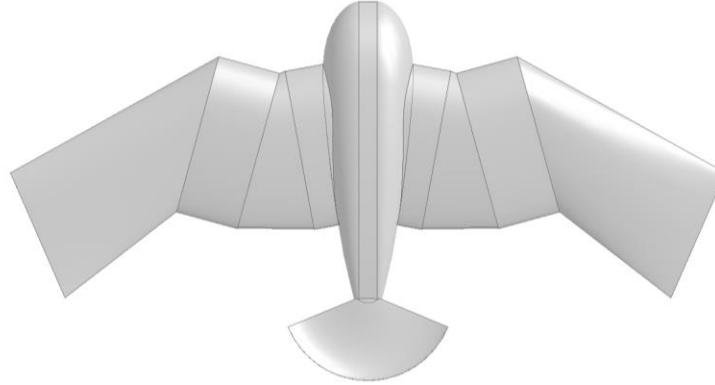


**Fig. 5. Simplified model of BIRD, fully tucked wing configuration**

The geometries, once imported into Ansys DesignModeler were surrounded by an enclosure measuring 1.3m in all directions except for the direction behind the drone model which was elongated at a 3.5m to account for backflow. At this time, symmetry could be applied if desired by splitting the model.

The intention was to simplify the model in this manner in order to more easily obtain convergence, but unfortunately, the models still presented a host of issues. These models, with their default meshes unaltered, still provided divergent results, but properly meshing the models using various mesh controls still did not provide an avenue for convergent results. At times the mesh would fail, presumably due to issues related to the generation of the mesh on this series of simplified models. Thus, no usable results were able to be obtained from these models. Since the geometries of different models may have their own specific problems that do not lend themselves to meshing well, all that can be generally concluded is that further work would have to be done on each specific model regarding the applications of mesh controls, as well as any other appropriate mesh generation techniques such as the use of mesh controls.

The mathematical model used in the Ansys fluent solver was the SST k-omega model. Simulations were performed with an inlet air velocity of around 12.07m/s.

### **III. Model Description**

The CAD assembly of BIRD is shown in **Fig.6**. Its fuselage houses the drone's internal components and is covered by a carbon fiber laminated outer shell. Three bulkhead structures are placed at different locations within the fuselage to provide support. Two servomotors secured inside the fuselage control the coupled sweeping motion of the middle and outer segments of the left and right wings. Another servomotor housed in the wrist joint controls the pitch of the outer wing section. An elastic band mechanism allows for passive feather expansion/retraction during wing sweep. At the rear of the fuselage, the tail bracket is assembled onto the rear bulkhead, where two additional servomotors control tail pitch and tilt morphing. To maintain stability of the morphing wings, the wing chord length was maintained at 0.29 m.

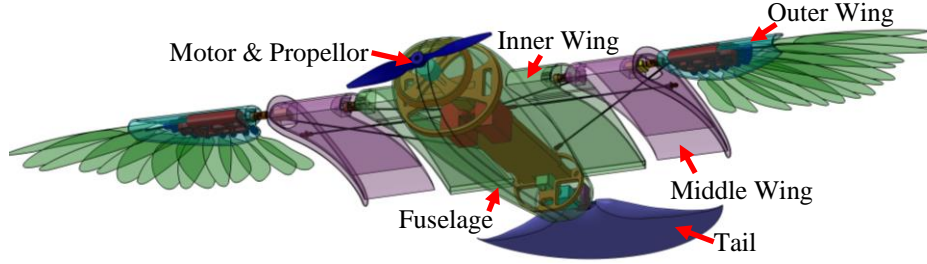


**Fig. 6. BIRD full CAD assembly**

#### **A. Wing Design**

**Fig. 7a** shows BIRD's wing design assembly. It achieves sweep morphing via three coupled degrees of freedom that mimic the movement of the gull's humerus, ulna, and carpometacarpus. The wing is divided into three segments: inner, middle, and outer segments. A shoulder joint housed within the fuselage is connected to the inner wing segment. This segment is supported by the fuselage structure to provide structural stiffness to the whole wing. An elbow joint connects the inner and middle wing segments, whereas a wrist joint connects the outer and middle wing segments. Selig 1223 airfoil profile was used in the inner and middle wing sections; the integrated inner wing was manufactured using carbon fiber while the middle and outer wing were both 3D-printed using PLA Aero. The outer wing segment includes 12 fiberglass feathers, each having a 2.5 mm diameter carbon fiber shaft supporting a carbon fiber feather vane. To increase the surface area, some feathers have 2 or 3 vanes supported by one shaft. This also adds some overlap between the feathers for additional support and flutter prevention. All feather shafts are connected to small feather joints housed in the outer wing's 3D-printed carpometacarpus bone. This bone is covered by a 3D-printed outer wing cover. Elastic bands are used to maintain the feather's relative position. A HS08A HV servomotor is used to control the sweep morphing of each wing. This servomotor is located inside the fuselage in special housing. One side of its horn is connected to the middle wing actuation rod, while the other side is connected to the shoulder joint in the inner wing via another rod. When the wing sweep morphing is applied, this servomotor pushes the middle wing. The outer wing actuation rod connects the inner and outer wing segments. Feather retraction is achieved passively during the sweepback motion of the outer wing via the outer wing actuation rod, which is connected to the middle wing segment and restricts the motion of the innermost feather to tuck the feathers closer together. Feather expansion is achieved through the elasticity of the tendons that connects all feathers and brings them back to their expanded configuration. Feather holders and the hinge sections attached to the leading edge of the wings are 3D-printed of PLA Aero. The sweep morphing leads to a 15% reduction in wing area.

Ajanic *et al.* [17] concluded that asymmetric wing pitch is more effective in generating roll moment than wing asymmetric sweep, and recommended pitching the wing outer wing segment, rather than the whole wing. Accordingly, only BIRD's outer wing segment has the pitch morphing capability. The pitch servomotor is A08 KST, and is located within the wrist joint, as shown in **Fig. 7a**.



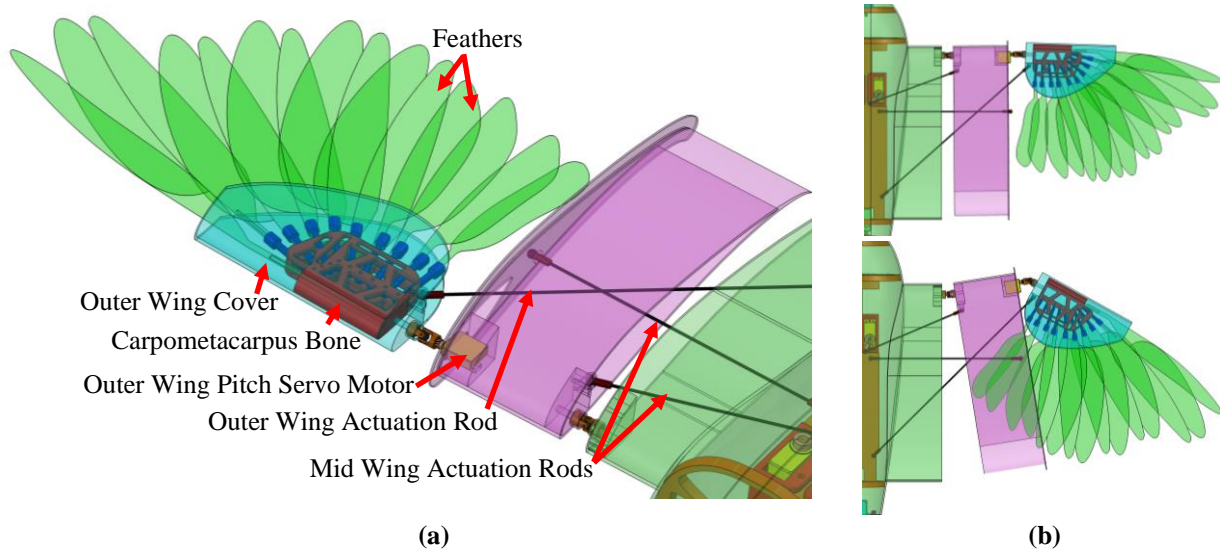


Fig. 7. (a) BIRD's wing design, (b) Wing expanded and tucked configurations

### B. Tail Design

BIRD's tail is shown in **Fig. 8a**. It has two degrees-of-freedom, tail pitch and tail tilt, similar to CGull's tail [22,23]. However, the tail structure on BIRD is not just a flat plate but has a Selig 1223 airfoil profile to aid in generating forces and moments for stability and maneuverability. The chord length is 30 cm which is equal to the average Western Gull's tail feather length [24]. The tail spread angle is  $135^\circ$  which is equivalent to fully spread tail feathers. The structure is made of Bambu Labs' PLA Aero for the main body with added Bambu's PLA CF along the central section of the tail for added stiffness and rigidity. An extruded lip is added to act as a mounting tab for the tail bracket. The tail bracket was created using Autodesk Fusion's Generative Design (**Fig. 8b**) with a target minimum factor of safety of 2. The tail bracket sandwiches the structure's lip between two extruded sections on the bracket, as shown in **Fig. 8a**, and are secured in place with two screws. Actuation is achieved via HTS-20H and LDX-218 servomotors, assembled in series, that pitch and tilt the tail, respectively. A servo holder that houses the HTS-20H servomotor is used to connect the tail assembly to the rear bulkhead of the fuselage.

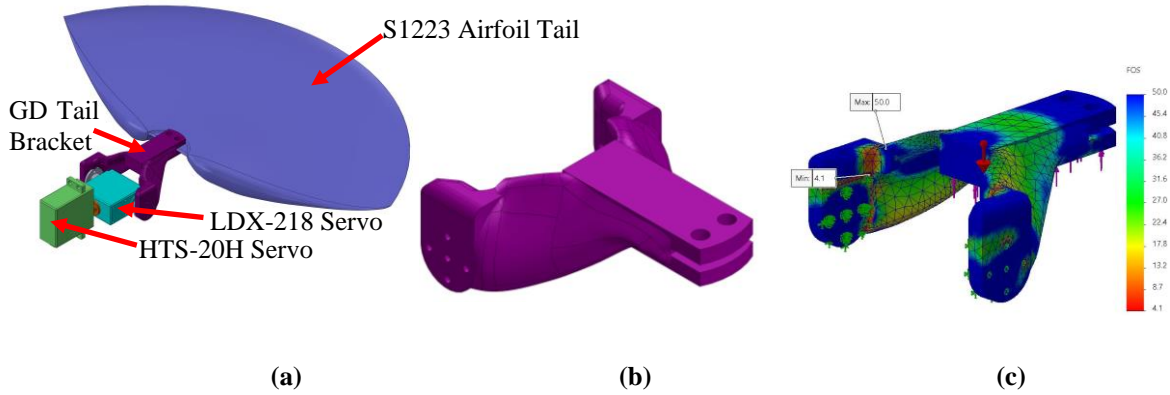


Fig. 8 (a) Tail assembly, (b) Generatively designed tail bracket and (c) its factor of safety plot

The generatively designed tail bracket was originally 3D-printed polyethylene terephthalate glycol (PETG), but through further research and testing, polylactic acid infused carbon fiber filament (PLA CF) from Bambu Labs was a more viable and durable option. It was designed to withstand a maximum aerodynamic force of  $22.7 \text{ kg}_f$  (50 lbs). Within the GD model, the tail bracket was adjusted to preserve sections of the bracket where the servomotors and tail are to be connected. While researching the properties of thermoplastics, their application via FEA were challenging as many thermoplastics lack the necessary properties (tensile strength, yield strength, etc.) that are needed for basic FEA studies (Stress, strain and factor of safety). Manufacturer's test data (i.e. Bambu Labs) and resource catalogues (i.e. MatWeb)



helped with determining or assuming the values like tensile strength or yield strength that will be utilized for the FEA study of the generative design tail bracket. After performing a convergence study, a blended curvature-based mesh was used to validate the GD study in a static analysis. **Fig. 8c** shows the factor of safety distribution on the bracket, and the minimum factor of safety was found to be 4.1. The difference between this value and the target minimum factor of safety in the GD tool comes from the slight geometric changes that happen to the GD parts when exported as CAD parts. The orientation of how forces are applied and the orientation of the layers of the thermoplastic determine the safety of the part as for tests that were applied along the X and Y plane (forces running perpendicular to the layer orientation), they showcased the strongest factors of safety. While if forces ran along the Z plane (running parallel with layer orientation), their factor of safety would be lessened or weaker.

### C. Fuselage Design

The fuselage structure, shown in **Fig. 9a**, includes three internal bulkheads made of 3D-printed Carbon-Fiber PLA. The front bulkhead serves as the mounting point for the motor, with the motor shaft passing through a hole at the nose of the fuselage outer shell to connect to the propeller. The middle and rear bulkheads support the avionics tray, where the flight control components are mounted. Additionally, the tail bracket is mounted on the rear bulkhead. The fuselage is horizontally split, providing easy access to the internal components. The fuselage skin is made of a 2-ply carbon fiber laminate with two integrated wings, as shown in **Fig. 9b**, to enable the middle wing sections to tuck into the inner wing during sweep morphing. These integrated wings have a Selig 1223 airfoil profile, but with the trailing edge simplified for easier manufacturing.

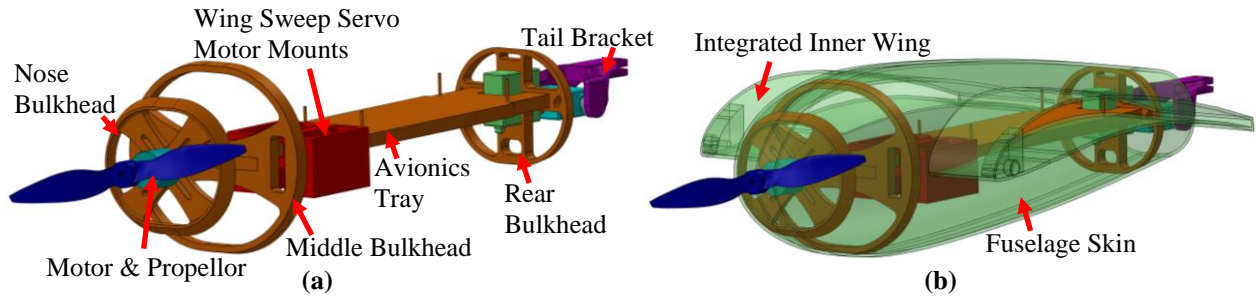


**Fig. 9. (a) Fuselage internal structure, (b) Fuselage skin with cutouts**

## IV. Avionics and Propulsion

BIRD's avionics system centers around the F405-Wing V2 flight controller, which manages flight stabilization, sensor integration, and control of the morphing wing mechanism. The flight controller connects to a FrSky X8R receiver, which communicates via radio frequency to the FrSky Taranis Qx7 controller, shown below in **Fig. 10**, for manual operation. The flight controller connects to Mission Planner software for real-time monitoring, and Data collection. The full Avionics and Propulsion System is shown in **Fig. 11**.



**Fig. 10. Remote Control Configuration**

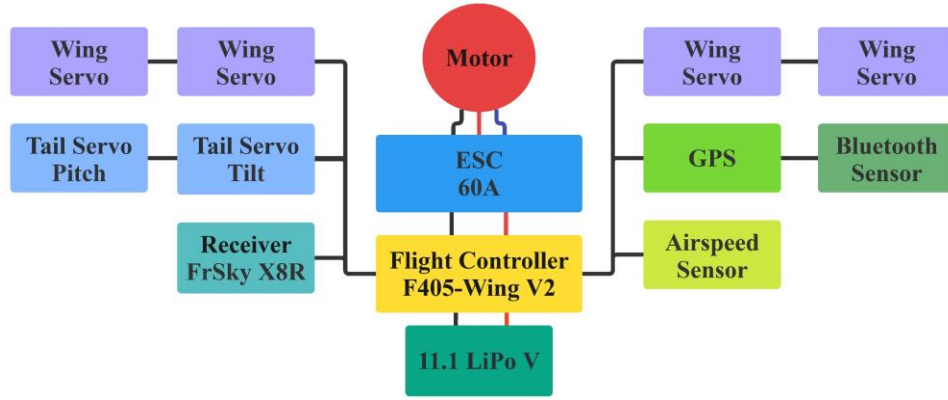


Fig. 11. Avionics System Flow Diagram

### A. Propulsion System

The propulsion system consists of a brushless DC motor (SunnySky X2216) and a  $9 \times 6$  nylon propeller, delivering sufficient thrust for steady flying. An electronic speed controller (ESC) rated at 60A regulates power flow from a high capacity 3S LiPo battery 2200 mAh, providing peak motor performance. The flight controller manages throttle controls and distributes power to all avionics components. This configuration provides a reliable and effective power source capable of performing morphing flight operations.

### B. Sensor System

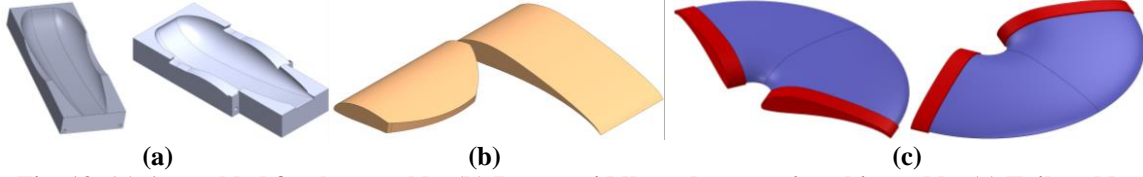
BIRD is equipped with a set of sensors used to improve data collecting and navigation. The flight controller is equipped with an ACEIRMC HC-06 RS232 Bluetooth module for wireless telemetry, a FrSky PAS70 ADV Air Speed Sensor for real-time airspeed readings, and an Ublox NEO-6M GPS module for accurate location. Additionally, a current sensor is used to track efficiency and power usage. Through this sensor system, BIRD can gather flight data, such as lift, drag, and velocity. When linked to a computer, live data is examined using Mission Planner software. This enables an analysis of changing wing dynamics and offer data on aerodynamic performance. Below is a screenshot of the telemetry data shown in Fig 12.



Fig. 12. Screenshot of Live Telemetry Data

## V. Manufacturing

Wet layup composite technique was used to manufacture the fuselage of BIRD. The wet layup is preferable for this structure due to the curvatures of the surface. The fuselage was split into two parts horizontally which allowed for female molds of the upper and lower parts of the fuselage to be created, as shown in **Fig. 13a**. Each of the molds was then divided into pieces that were 3D-printed and assembled using bolts. 3D-printing the molds allows for easy release once the cure process is completed, as the molds can be easily disassembled. To improve the surface finish, the gaps in the mold were filled with Bondo filler to smoothen the surface, and a final coating of Duratec polyester surface primer was added. Additionally, the final preparation of the mold consisted of wet sanding at various grit and six coats of mold release wax to help with releasing the manufactured part once the cure cycle is completed. **Fig. 14a** shows the manufactured and assembled fuselage molds. Two woven carbon-fiber plies were used to construct the fuselage in the wet-layup process.



**Fig. 13. (a) Assembled fuselage molds, (b) Inner, middle and outer wing skin molds, (c) Tail molds**

The wings were designed using Selig 1223 airfoils and 3D-printed for the two segments of the wing and the tail structure, as shown in **Fig. 13b, c** (CAD designs) and **Fig. 14b** (manufactured models). During the layup, an extended trailing edge was left to separate the upper and lower surfaces, allowing for easier part release. The inner and middle wing skin shells were created from the same mold since they have the same profile and length. Wet-layup composite technique was also used to manufacture these structures, and two woven carbon fiber plies were enough to construct sturdy structures. Once curing was completed and the parts were released from the molds, the edges of the parts were trimmed, and the skin sections were then cut to their desired sizes. The upper and lower surfaces were then bonded at the trailing edge and each skin section was covered with a coat of resin sealer to give a gloss finish.

The wing and tail structures were all 3D printed using PLA Aero and PLA Carbon Fiber. The carbon fiber filament would be added to the structures to add stability for the Aero filament. PLA Aero can be prone to stringing defects, the stability of the carbon fiber added a base for the Aero filament to print properly while strengthening areas of the structures. PLA Aero contains air pockets within the filament which expand once heated for printing. This heating causes the material to foam which creates a lighter more porous structure compared to regular PLA. Changing to PLA Aero had allowed for more than 40% weight reduction compared to previous iterations of airfoils manufactured out of carbon fiber.

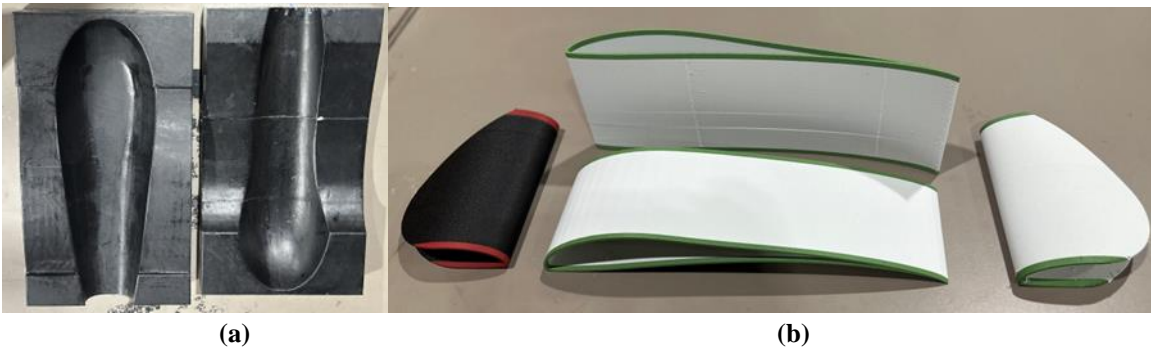


**Fig. 14. (a) 3D-printed top and bottom fuselage molds, (b) 3D-printed structures for wing segments**

The feathers were manufactured using two plies of CYCOM 5350 woven fiberglass prepreg that sandwich 2.5 mm diameter carbon fiber rods which act as feather shafts. A single ply would act as the entire feather, while a singular strip would only reinforce the shaft area. The shaft extends through the entire feather to add stability during flight. A flat tempered glass plate was used as a mold where the cure cycle was then followed within an industrial oven. The avionics

tray was cut from a sandwich composite panel that has one ply in each face plate and a 5 mm honeycomb thick Nomex core. All other components were 3D-printed and assembled. All wing and tail servomotors were also mounted. The total weight of the fuselage with all avionics components was 850 g, while the weight of the tail subassembly is 150 g. The total weight of BIRD prototype is 1880 g.



**Fig. 15. (a) Composite structures: fuselage, (b) 3D-Printed PLA Aero Tail Structure**

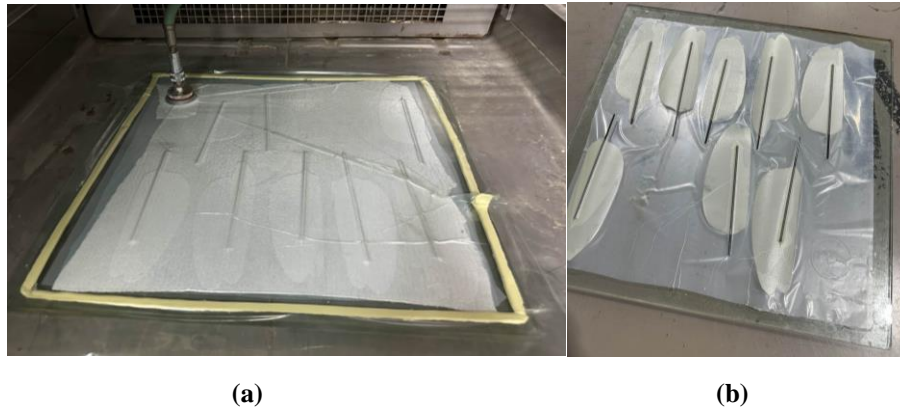


**Fig. 16. (a) Fiberglass composite feathers in oven, (b) Fiberglass feathers after curing**

## VI. Testing

### A. Actuation Testing

Wing actuation testing is shown in **Fig. 17**, while tail actuation is shown in **Fig. 18**. All selected servomotors proved to be capable of actuating the morphing mechanisms efficiently.

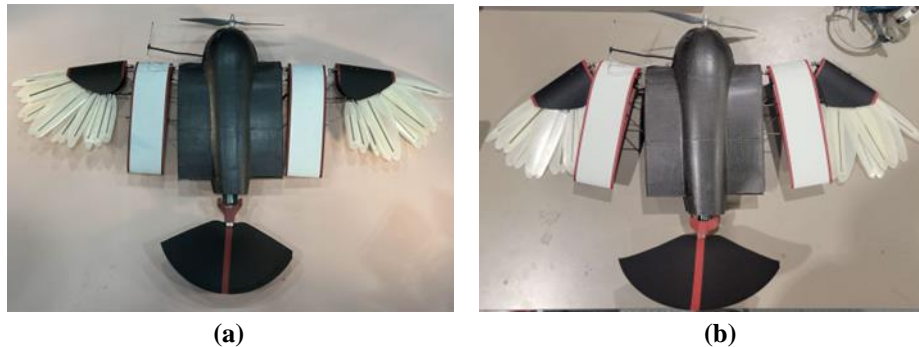


**Fig. 17 BIRD prototype in (a) Fully expanded configuration, and (b) fully tucked configuration**



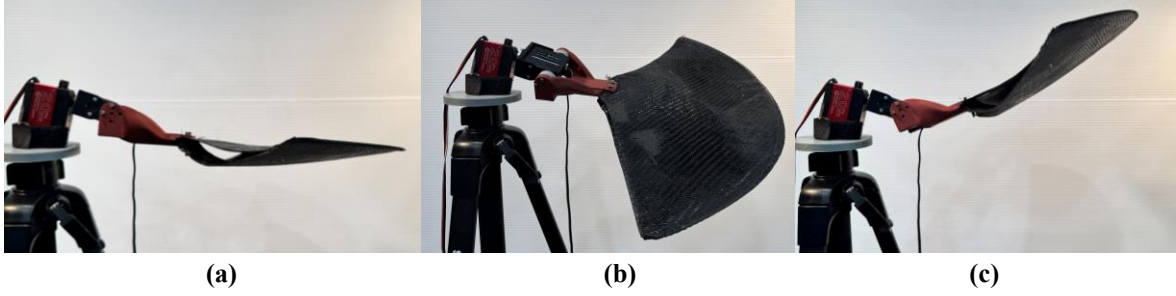


**Fig. 18 (a) Tail neutral configuration, (b) Tail tilted configuration, (c) Tail pitch down configuration**

### B. Wind Generator

A multi-fan wind generator, named Zephyrus, was designed to test the drone's wing and tail subassemblies under aerodynamic loads. The mini version of this drone includes only three modules, as shown in **Fig. 19a**, and has a test section of  $83.8 \text{ cm} \times 27.9 \text{ cm}$ . It utilizes counter-rotating fans for clean airflow, distributed power loads across multiple power supplies, and Arduino microcontrollers for synchronized fan control and data acquisition. Counter-rotating fans minimize turbulence by canceling rotational effects, ensuring high static pressure and uniform airflow, which is crucial for aerodynamic testing. Each fan module has a 3D-printed frame with four spokes to mount the motors, as shown in **Fig. 19b**, two propellers, ESCs, Arduino controllers, and metal bracket hardware. The first rotor has 5 blades and is used to build pressure efficiently and impart a controlled swirl, while the second rotor has 3 blades and is used to capture and redirect the flow, straightening it. This reduces turbulence, improves laminarity, and increases efficiency in the wind tunnel. This is further supported by **Fig. 20** where airspeed measurements with an anemometer showed that the counter rotating blades of a single module produced twice as much airflow compared to a single blade [25]. Since the motors generate heat while in operation, mounting metal x-brackets with rods were fabricated and installed to mitigate heat transfer from the motors to the 3D-printed frame and prevent warpage of the plastic structures. Preliminary testing proved that the module could reach an air speed of  $15.65 \text{ m/s}$  ( $35 \text{ mph}$ ), with only 70% of its power capacity. **Fig. 21** shows the manufactured prototype, which includes the power distribution system (PDS) made up of powers supplies, Arduino micro controller, shutoff relay and emergency stop. A protective mesh screen was added to ensure test model and user safety.

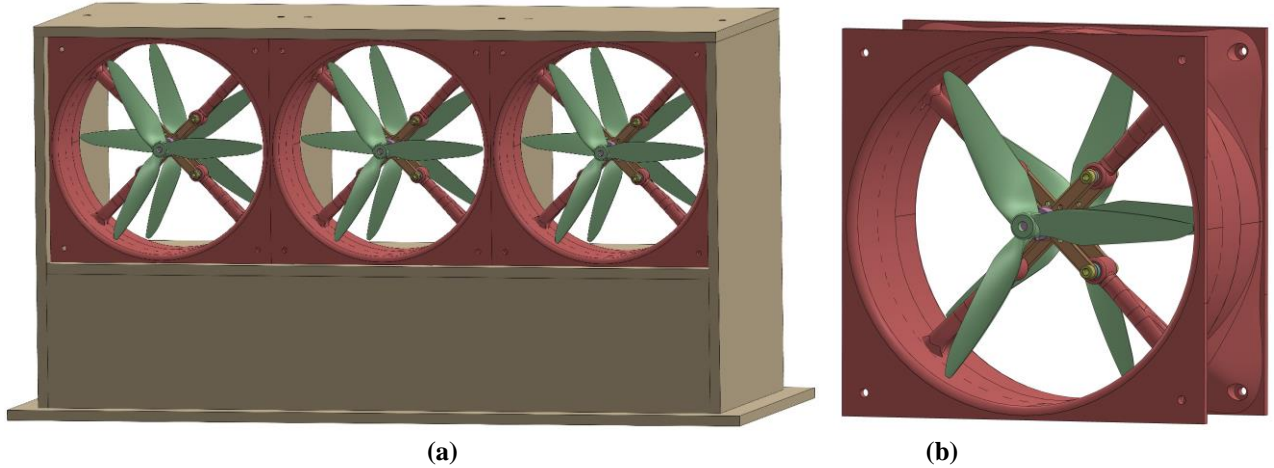


**Fig. 19. (a) Zephyrus Mini, (b) Fan module close up**

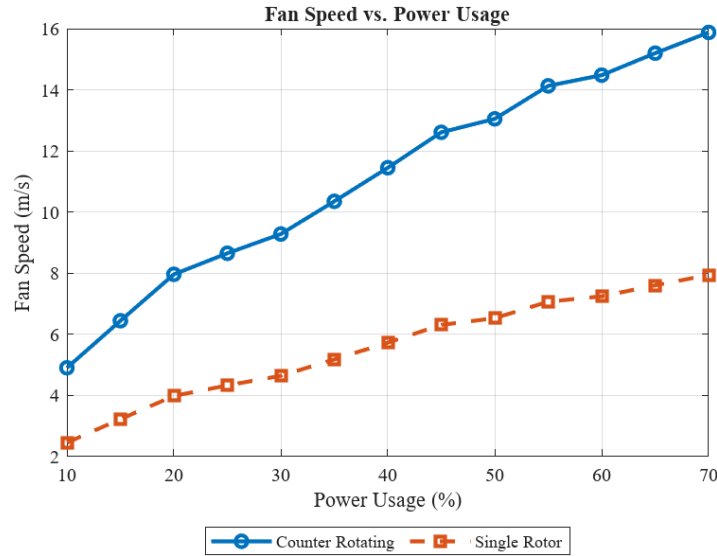


**Fig. 20. Air speed measurements of blade configurations**



(a)



(b)

**Fig. 21. Manufactured model: (a) Front view, (b) rear view**

A versatile control interface, shown in **Fig. 22**, was developed in the Arduino IDE to regulate fan motor speeds based on power supply loading, ranging from 10% to 70% to prevent system overload and maintain a 30% safety margin. Each of the three modules can be controlled independently, allowing precise flow control across different sections, with selectable presets for stable and unstable airflow. An emergency shutoff button was also included. The interface operates through an Arduino ESP32, enabling users to connect over Wi-Fi using the chip's assigned IP address.

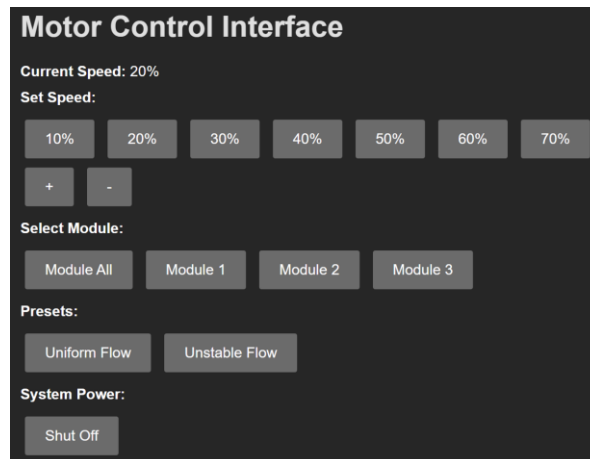


**Fig. 22. Arduino Control Interface**



Tests were performed by securing the manufactured outer feathered wing segment on a tripod and placing it in front of the Zephyrus Mini operating at varying air speeds up to 15.6 m/s, as shown in . Carbon fiber was initially chosen for the feathers due to its stiffness, but the material proved too heavy despite exhibiting minimal deflection (**Fig. 23a**). To reduce weight, a hybrid design using balsa wood and carbon fiber was tested, which lowered mass but introduced significant flutter issues (**Fig. 23b**). Ultimately, fiberglass feathers were fabricated and successfully met both weight and flutter performance requirements (**Fig. 23c**). Similarly, under the highest expected aerodynamic loads, the wing remained sturdy at various AOAs and exhibited minimal deflection or oscillatory behavior, confirming its structural adequacy during actuation.

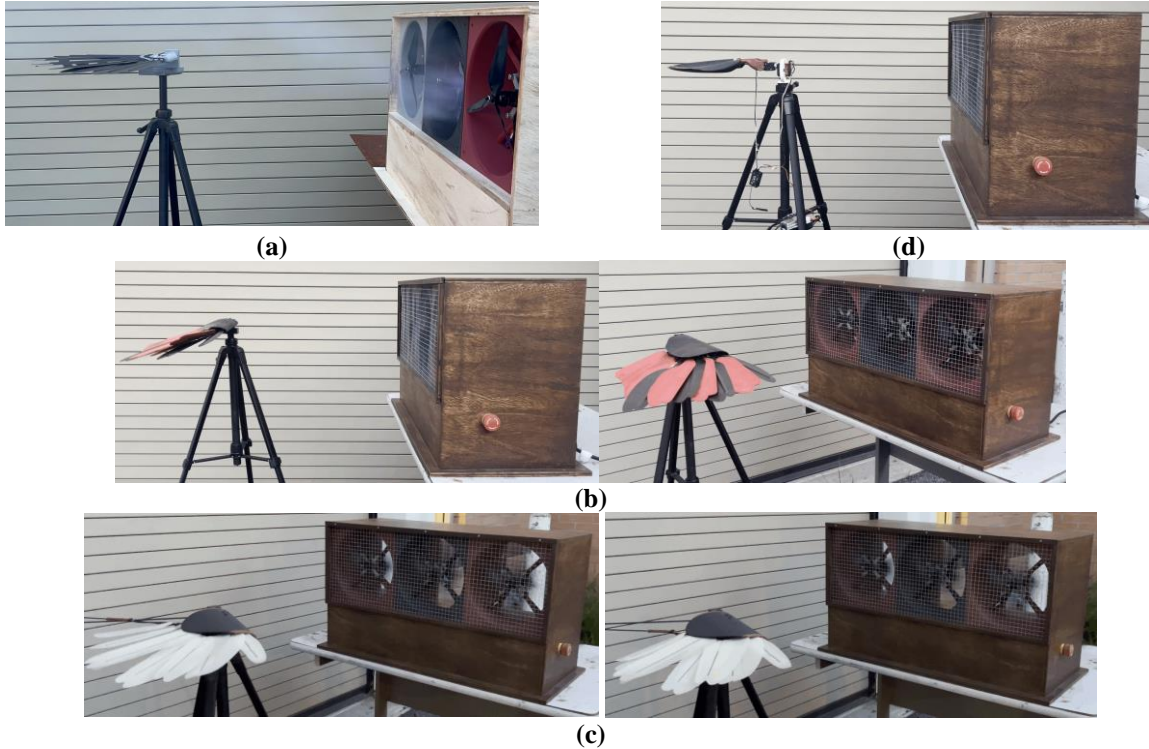


**Fig. 23 Multi-fan wind generator tests for outer feathered wing (a) fully carbon fiber, (b) balsa and carbon fiber, (c) fiberglass, and (d) tail subsystem.**

Similarly, the tail subsystem was tested, as shown in **Fig. 23d**. The pitch and tilt servomotors were able to actuate the tail structure properly and the structure remained sturdy at various tail pitch and tilt angles.

### C. Thrust Testing

A thrust stand, shown in **Fig. 24a**, was designed to measure the thrust force and motor RPM of the brushless motors used in the drone and the wind generator with different propeller sizes. A load cell was fitted to the system to properly measure the thrust force produced by each motor-propeller combination. The manufactured and assembled stand is shown in **Fig. b**. During testing, each motor was operated at different throttle settings where both thrust, and RPM data were collected. These experiments gave data for determining the best propulsion arrangement for BIRD.

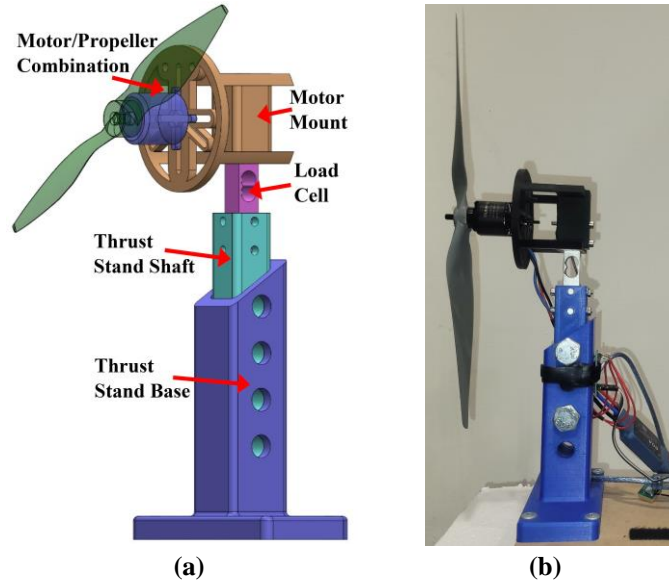


**Fig. 24. Thrust stand (a) CAD model, (b) manufactured and assembled model**

## **VII. Summary and Conclusion**

This paper presents the design of BIRD, a bio-inspired non-flapping UAV, that combines wing sweep morphing along with wingtip pitch morphing and features a significant number of composite structures. A numerical model was first developed in MachUpX to understand the effects of the various morphing degrees-of-freedom on the generated aerodynamic forces and moments. Prototypes of all subsystems were manufactured and assembled. A multi-fan wind generator and a thrust stand were designed and manufactured to test the manufactured prototypes under aerodynamic loads and confirm the ratings of the selected motors, respectively. Actuation tests were performed to validate the design choices and prepare BIRD for flight tests to follow.

## **Acknowledgments**

This work was done by the ninth cohort of the “Smart Morphing Wing” research-based senior design project at California State University, Northridge (CSUN). The authors acknowledge the Mechanical Engineering Department, the Instructionally Related Activities (IRA) grant, and the Student Travel and Academic Research (STAR) program at CSUN.

## References

- [1] Kidd, S. M., “The Invention of Wings,” Penguin Books, New York, New York, 2015.
- [2] McCullough, D. G., “The Wright Brothers,” Simon & Schuster, Riverside, 2015.
- [3] Jakab, P. L., “Otto Lilienthal: ““The Greatest of the Precursors,”” *AIAA Journal*, Vol. 35, No. 4, 1997, pp. 601–607. <https://doi.org/10.2514/2.154>
- [4] Han, J., Hui, Z., Tian, F., and Chen, G., “Review on Bio-Inspired Flight Systems and Bionic Aerodynamics,” *Chinese Journal of Aeronautics*, Vol. 34, No. 7, 2021, pp. 170–186. <https://doi.org/10.1016/j.cja.2020.03.036>
- [5] Han, J.-H., Han, Y.-J., Yang, H.-H., Lee, S.-G., and Lee, E.-H., “A Review of Flapping Mechanisms for Avian-Inspired Flapping-Wing Air Vehicles,” *Aerospace*, Vol. 10, No. 6, 2023, p. 554. <https://doi.org/10.3390/aerospace10060554>
- [6] Ameduri, S., and Concilio, A., “Morphing Wings Review: Aims, Challenges, and Current Open Issues of a Technology,” *Proceedings of the Institution of Mechanical Engineers, Part C: Journal of Mechanical Engineering Science*, Vol. 237, No. 18, 2023, pp. 4112–4130. <https://doi.org/10.1177/0954406220944423>
- [7] Harvey, C., Gamble, L. L., Bolander, C. R., Hunsaker, D. F., Joo, J. J., and Inman, D. J., “A Review of Avian-Inspired Morphing for UAV Flight Control,” *Progress in Aerospace Sciences*, Vol. 132, 2022, p. 100825. <https://doi.org/10.1016/j.paerosci.2022.100825>
- [8] Harvey, C., and Inman, D. J., “Aerodynamic Efficiency of Gliding Birds vs Comparable UAVs: A Review,” *Bioinspiration & Biomimetics*, Vol. 16, No. 3, 2021, p. 031001. <https://doi.org/10.1088/1748-3190/abc86a>
- [9] Harvey, C., and Inman, D. J., “Gull Dynamic Pitch Stability Is Controlled by Wing Morphing,” *Proceedings of the National Academy of Sciences*, Vol. 119, No. 37, 2022, p. e2204847119. <https://doi.org/10.1073/pnas.2204847119>
- [10] Kilian, L., Shahid, F., Zhao, J.-S., and Nayeri, C. N., “Bioinspired Morphing Wings: Mechanical Design and Wind Tunnel Experiments,” *Bioinspiration & Biomimetics*, Vol. 17, No. 4, 2022, p. 046019. <https://doi.org/10.1088/1748-3190/ac72e1>
- [11] Murayama, Y., Nakata, T., and Liu, H., “Aerodynamic Performance of a Bird-Inspired Morphing Tail,” *Journal of Biomechanical Science and Engineering*, Vol. 18, No. 1, 2023, pp. 22-00340-22-00340. <https://doi.org/10.1299/jbse.22-00340>
- [12] Li, J.-H., Sun, H.-L., De Reydet De Vulpillières, Y., Wang, Z.-Y., and Zhao, J.-S., “A Bionic Morphing Tail Mechanism for Aerial Vehicles,” presented at the 2024 6th International Conference on Reconfigurable Mechanisms and Robots (ReMAR), Chicago, IL, USA, 2024. <https://doi.org/10.1109/ReMAR61031.2024.10618010>
- [13] Gamble, L. L., and Inman, D. J., “A Tale of Two Tails: Developing an Avian Inspired Morphing Actuator for Yaw Control and Stability,” *Bioinspiration & Biomimetics*, Vol. 13, No. 2, 2018, p. 026008. <https://doi.org/10.1088/1748-3190/aaa51d>
- [14] Di Luca, M., Mintchev, S., Heitz, G., Noca, F., and Floreano, D., “Bioinspired Morphing Wings for Extended Flight Envelope and Roll Control of Small Drones,” *Interface Focus*, Vol. 7, No. 1, 2017, p. 20160092. <https://doi.org/10.1098/rsfs.2016.0092>
- [15] Hui, Z., Zhang, Y., and Chen, G., “Aerodynamic Performance Investigation on a Morphing Unmanned Aerial Vehicle with Bio-Inspired Discrete Wing Structures,” *Aerospace Science and Technology*, Vol. 95, 2019, p. 105419. <https://doi.org/10.1016/j.ast.2019.105419>
- [16] Ajanic, E., Feroskhan, M., Mintchev, S., Noca, F., and Floreano, D., “Bioinspired Wing and Tail Morphing Extends Drone Flight Capabilities,” *Science Robotics*, Vol. 5, No. 47, 2020, p. eabc2897. <https://doi.org/10.1126/scirobotics.abc2897>
- [17] Ajanic, E., Feroskhan, M., Wüest, V., and Floreano, D., “Sharp Turning Maneuvers with Avian-Inspired Wing and Tail Morphing,” *Communications Engineering*, Vol. 1, No. 1, 2022, p. 34. <https://doi.org/10.1038/s44172-022-00035-2>
- [18] Chang, E., Matloff, L. Y., Stowers, A. K., and Lentink, D., “Soft Biohybrid Morphing Wings with Feathers Underactuated by Wrist and Finger Motion,” *Science Robotics*, Vol. 5, No. 38, 2020, p. eaay1246. <https://doi.org/10.1126/scirobotics.aay1246>
- [19] Chang, E., Chin, D. D., and Lentink, D., “Bird-Inspired Reflexive Morphing Enables Rudderless Flight,” *Science Robotics*, Vol. 9, No. 96, 2024, p. eado4535. <https://doi.org/10.1126/scirobotics.ado4535>
- [20] Brody, M., Podell, D., Corte Garcia, F., Munoz, E., Massey, S., Minassian, E., Gharibi, N., Lyon, D., Sanchez, B., and Bishay, P. L., “MataGull: A Lightweight Bio-Inspired Non-Flapping Bird-like Morphing Drone,” presented at the 2023 Regional Student Conferences, Region I - North East, University at Buffalo, Buffalo, New York, United States of America, 2023. <https://doi.org/10.2514/6.2023-72218>
- [21] Bishay, P. L., Brody, M., Podell, D., Corte Garcia, F., Munoz, E., Minassian, E., and Bradley, K., “3D-Printed Bio-Inspired Mechanisms for Bird-like Morphing Drones,” *Applied Sciences*, Vol. 13, No. 21, 2023, p. 11814. <https://doi.org/10.3390/app132111814>
- [22] Bishay, P., Rini, A., Brambila, M., Niednagel, P., Eghdamzami, J., Yousefi, H., Herrera, J., Saad, Y., Bertuch, E., Black, C., Hanna, D., and Rodriguez, I., “CGull: A Non-Flapping Bioinspired Composite Morphing Drone,” *Biomimetics*, Vol. 9, No. 9, 2024, p. 527. <https://doi.org/10.3390/biomimetics9090527>
- [23] Hanna, D., Rini, A., Eghdamzami, J., Saad, Y., Arias-Rodas, A., Brambila, M., Yousefi, H., Black, C., Herrera, J., and Bishay, P., “Design of a Non-Flapping Seagull-Inspired Composite Morphing Drone,” presented at the AIAA SCITECH 2025 Forum, Orlando, FL, 2025. <https://doi.org/10.2514/6.2025-0124>
- [24] Dunn, J. L., Alderfer, J. K., and National Geographic Society (U.S.), Eds., “National Geographic Field Guide to the Birds of North America,” National Geographic, Washington, D.C, 2017.
- [25] Tang, Z., Liu, P., Chen, Y., and Guo, H., “Experimental Study of Counter-Rotating Propellers for High-Altitude Airships,” *Journal of Propulsion and Power*, Vol. 31, No. 5, 2015, pp. 1491–1496. <https://doi.org/10.2514/1.B35746>